

Electromechanical Actuator Ribbons Driven by Electrically Conducting Spring-Like Fibers

Peining Chen, Sisi He, Yifan Xu, Xuemei Sun, and Huisheng Peng*

Electromechanical actuators that convert electric energy into mechanical energy have recently attracted increasing attentions due to their promising applications such as artificial muscles, microrobots, sensors, and biomimetic devices.^[1–6] Among them, the electrothermally, electrochemically, and electrostatically layered actuators based on an asymmetric expansion between the neighboring layers are mostly explored for a bending deformation.^[7–12] More specifically, an electrothermally driven bimorph actuator reversibly bends or unbends as the thermal expansion coefficients of two contacted layers were mismatched;^[7,13] an electrochemical trilayer actuator, consisting of an electrolyte layer laminated by two electrode layers, generates a bending motion as a result of the shrinkage/expansion of electrode layers caused by ion migrations under the electric field;^[8,10] an electrostatically driven actuator produces a mechanical motion by the laminated polymeric membrane as a result of Coulomb force.^[14,15] The electromechanical actuators are generally made from ferroelectric ceramics, shape memory alloys, and electroactive polymers. Although some advantages have been claimed for these actuators, e.g., large actuation strains are observed for electrothermally and electrostatically driven actuators and low voltages are required for electrochemically driven actuators, there remain many challenges for each kind of actuator.^[10–12,16] Both slow responsiveness and weak cyclic life are shared for electrothermally and electrochemically driven actuators; limited electrolyte media work for electrochemically driven actuators; ultrahigh driving voltages are required for electrostatically driven actuators.

CNTs have been well recognized for combined remarkable properties such as high tensile strengths and electrical conductivities that may be further extended to the macroscopic scale based on a highly aligned structure in the continuous CNT fiber.^[17–20] The CNT fibers demonstrated tensile strengths of hundreds of megapascal and electrical conductivities of hundreds of Siemens per centimeter. In addition, intriguing electromagnetic interactions were found among aligned CNTs to offer promising electronic and actuating properties in energy harvesting/storage devices and actuators.^[21–24] The electromagnetic driven CNT actuators exhibit a high stress output of more

than 200 times that of typical skeletal muscle, accompanied with a rapid responsiveness and low operating voltage.^[25–27] In particular, compared with the previously reported electrothermally and electrochemically driven actuators,^[10,22,23] they are composed of bare aligned CNTs without any functional guest polymers or electrolytes, endowing them with high actuation stability and adaptability to various media (such as air, water and organic solution, etc.). The unique structures and distinguished properties had inspired us to investigate aligned CNT fibers as building blocks to prepare electromechanical actuator with hierarchical structures and enhanced actuation performances.

In this Communication, a new general and effective strategy has been developed to prepare single-layer fabric ribbons with tunable electromechanical actuations by integrating spring-like carbon nanotube (CNT) fibers that are flexible and mechanically robust through a sewing method. The resulting spring-like fibers (SLFs) exhibit superior electromagnetic actuation performances to the single ply CNT fibers including much higher contractive strain (14%) and greatly enhanced rotation output (135 revolutions per meter). The resulting fabric ribbon actuator generates remarkable bending/unbending electromechanical motions with rapid responsiveness and high reversibility. Interestingly, the ribbon actuator can be further made into helically 3D structures through a heat-setting method to exhibit programmable and rapid lengthwise elongation and contraction by tuning the chirality of the ribbon or SLFs.

To obtain the SLF, helically aligned CNT fibers were first prepared from spinnable CNT arrays that had been synthesized by chemical vapor deposition.^[28] The chirality of above fibers, i.e., left- and right-handedness, had been tuned by varying the spinning direction during preparation (Figures S1 and S2, Supporting Information). They were then bundled together in parallel and overtwisted into an SLF by stabilizing one end while rotating the other end. The bundled CNT fibers had been transferred into coiled loops along the axial direction after the inserting turns exceeded a critical value. Figure S3 (Supporting Information) shows a continuous SLF twisted from 20 left-handed CNT fibers, and micrometer-scale loops are closely packed with a left-handed chirality along the axial direction. Similarly, an SLF with right-handed loops had been also obtained after overtwisting a bundle of right-handed CNT fibers in a clockwise direction (Figure S4, Supporting Information). Importantly, these SLFs were mechanically stable and no entwisting or untwisting was observed in a relaxing state; thus, they could be further twisted into larger fibers to generate higher electromechanical actuations for practical applications (Figure 1).

Electromechanically contractive and rotary actuations had been simultaneously generated for the SLF upon the pass of

P. Chen, S. He, Y. Xu, Dr. X. Sun, Prof. H. Peng
State Key Laboratory of Molecular
Engineering of Polymers
Collaborative Innovation Center of Polymers
and Polymer Composite Materials
Department of Macromolecular Science and
Laboratory of Advanced Materials
Fudan University
Shanghai 200438, China
E-mail: penghs@fudan.edu.cn



DOI: 10.1002/adma.201501731

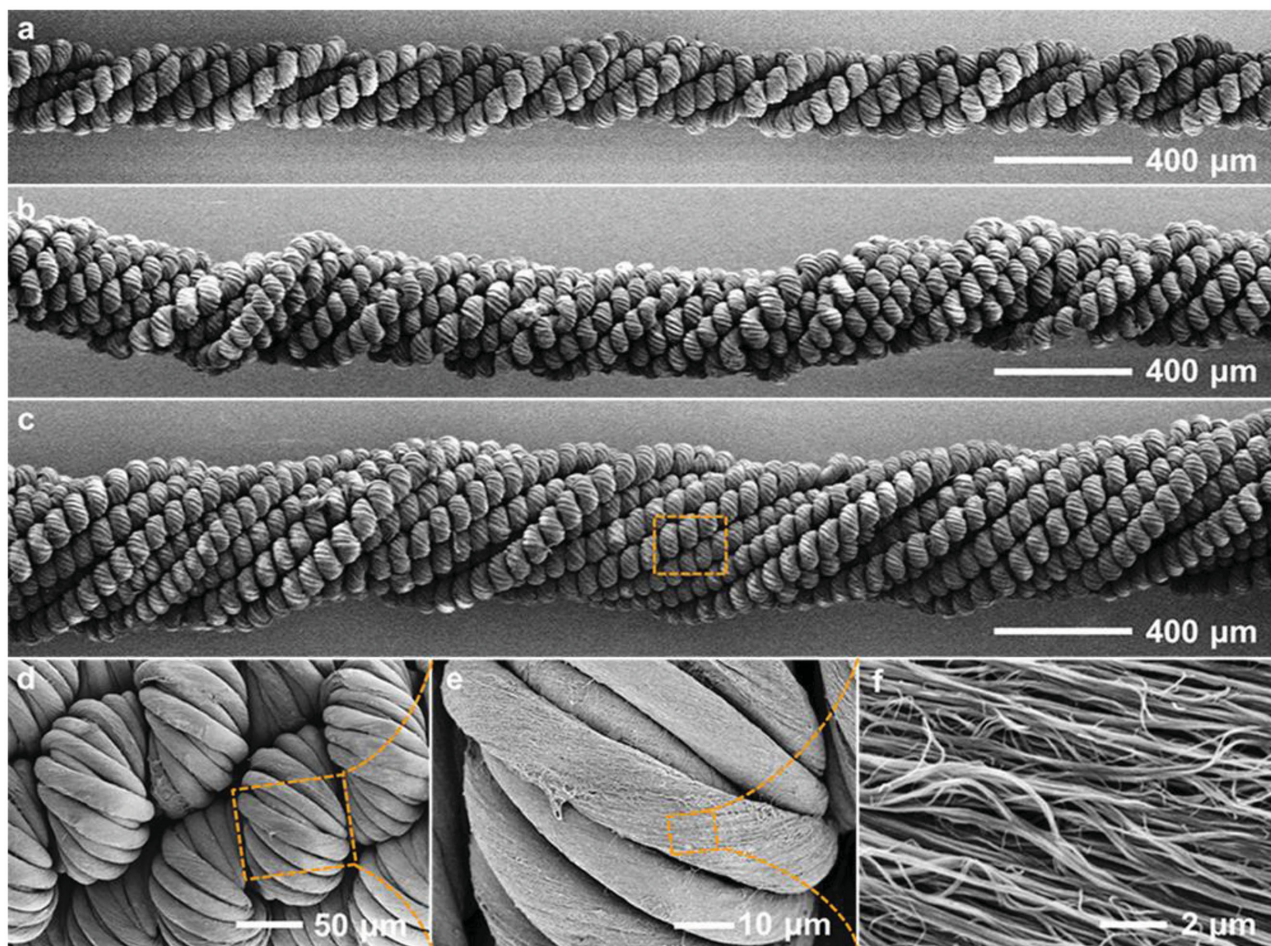


Figure 1. SEM images of twisted SLFs. a–c) Twisted 5, 10, and 20 left-handed SLFs, respectively. d) Enlarged image of (c). e) Enlarged image of (d). f) Enlarged image of (e).

an electric current. Figure S5 (Supporting Information) shows a typical contractive stress curve under a pulse current being applied on a SLF twisted from 20 left-handed CNT fibers. The SLFs could be triggered by pulse currents with a board range of frequencies, and the frequencies ranging from 0.25 to 2 Hz were mainly used in the following study to match the frequency of natural skeletal muscles (≈ 2 Hz). The generated contractive stress reached a plateau of 1.6 MPa, more than 16 times of the typical natural skeletal muscle.^[11] In particular, the electromechanical contraction had been rapidly completed within 160 ms, generating a maximal contractive stress rate of 20 MPa s⁻¹. Upon application of a linear electric current (Figure S6, Supporting Information), the generated contractive stress was gradually amplified to 1.6 MPa with the linearly increasing electric current. The relationship between contractive stress (F) and electric current (I) could be approximately expressed as $F \propto I^2$, which might be explained by the electromagnetic effects among the electrically conducting fibers,^[24–26] in consideration of the fact that a hierarchy of helical units, i.e., MWCNTs, primary fibers and loops exist in the SLF.

The contractive actuation could be enhanced by increasing the numbers of SLFs (Figure 1a–c). For instance, with

increasing SLF number, the maximal bearable powers and corresponding contractive forces were linearly increased and no obvious decays had been detected in the maximal contractive stress (Figure S7, Supporting Information). As expected, an electrothermal effect was additionally generated among the fiber during electromechanical actuation.^[29] The electromechanical actuation was highly reversible, and no obvious decrease was observed after 4000 cycles (Figure S8, Supporting Information) due to the excellent thermal stability of CNTs themselves. Additionally, the contractive stress could be accurately tuned by varying the current magnitude with high durability. For instance, the contractive stresses had been maintained at 0.33 and 1.00 MPa for over 30 min upon the use of electric powers of 75 and 272 mW to a large fiber twisted from 20 SLFs, respectively (Figure S9, Supporting Information).

The electromechanically rotary actuation generated by a left-handed SLF was recorded by a high-speed camera (Figure S10 and Movie S1 in the Supporting Information). The number of revolutions and rotary speed over time had been obtained through a frame-by-frame analysis (Figure S11, Supporting Information). When a pulse current (40 mA and

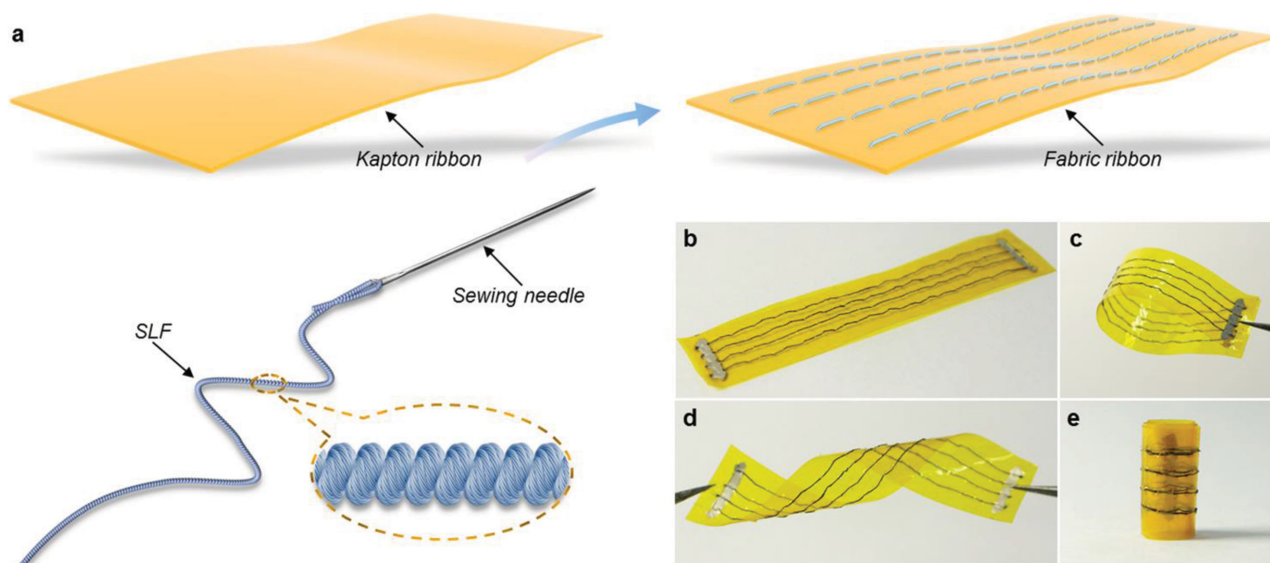


Figure 2. Preparation of Kapton fabric ribbon woven from SLFs. a) Schematic illustration. b) Photograph of a Kapton fabric ribbon. c–e) Photographs of fabric ribbon after bending c), twisting d), and rolling e), respectively. The ribbons shared a length of 4 cm and width of 1.2 cm.

2 Hz) was passed through a left-handed SLF twisted from 20 CNT fibers, an anticlockwise rotary actuation of 135 revolutions per meter had been generated within 250 ms, three orders of magnitude higher than the torsional actuators based on shape memory alloys, conducting polymers, and piezoelectric ceramics.^[30–32] In particular, the rotation output is 200 times higher than that of a single-ply CNT fiber.^[25] The great enhancement above may be attributed to the following reasons. First, the spring loops formed within SLFs make it more flexible than the single-ply fiber (Figure S12, Supporting Information), i.e., the former exerted a weaker drag force to the rotary actuation than the later; two, for an SLF upon pass of a current, the electromagnetic effects among the primary fibers and spring-loops might be additionally generated besides the electromagnetic effects preexisting among MWCNTs. In consequence, an enhanced rotation output was thus generated by the SLF. The rotary speed reached 978 rpm despite the fact that the mass of hanging metal paddle was more than 400 times of the SLF in weight. The initial torsional torque provided by the SLF was calculated as 1.11 N m kg^{-1} , which is comparable to the commercial electromagnetic motors.^[22] The above electromechanically rotary actuation was highly reversible and stable, and the revolutions were varied in less than 5% after actuations for 2000 cycles (Figure S13, Supporting Information). Additionally, the rotary direction could be tuned by varying the helical chirality of the SLF. In comparison to anticlockwise rotation generated by a left-handed SLF, a right-handed SLF generated a clockwise rotary actuation upon pass of an electric current.

The electromechanical actuations in contractive strain had been greatly enhanced compared with the building CNT fibers before coiled loops were formed. For instance, when passed with an electric current of 40 mA, a slack left-handed SLF twisted from 20 CNT fibers was rapidly stretched to be straight within 100 ms (Movie S2 and Figure S14 in the Supporting

Information) that was hundreds of times faster than typical actuators based on conducting polymers and ionic polymer–metal composites;^[8,10,11] the contractive strain of $\approx 14\%$ was more than 140 and ten times of those generated by the ferroelectric ceramics and single-ply CNT fiber, respectively.^[11,22,25] Due to the rapid and strong electromechanical contraction, a metal block with a mass of 70 mg (more than 330 times of the actuating fiber) had been lifted by 1.5 mm within 150 ms upon applying an electric current of 40 mA according to the experimental setup in Figure S15 (Supporting Information). The metal block was accelerated to a maximal ascending velocity of 41 mm s^{-1} during the initial 32 ms, providing a total power output of 77.7 W kg^{-1} . As expected, a reversible ascending and descending motion could be achieved by the SLF (Movie S3, Supporting Information).

The shape transformation of single-layer sheets triggered by external stimuli has been widely explored previously, though they are most made from elastomers or hydrogels with distinct mechanically responding behaviors.^[33–35] The SLFs are flexible and mechanically strong with a fracture strain of 245% and strength of 220 MPa, respectively (Figure S12, Supporting Information); thus, they could be woven into a commercially available Kapton film in parallel by using a sewing method (Figure 2a). A Kapton film served as the supporting substrate because it is commercially available, low-cost, and flexible. The two ends of the SLFs were then stabilized onto the Kapton ribbon by silver paste (Figure 2b). The resulting fabric ribbon was mechanically stable as it was subjected to bending and twisting treatments (Figure 2c,d), and it could be readily rolled up without obvious structural damages (Figure 2e). Additionally, the SLFs could also be woven into the Kapton films with optional sewing patterns such as square, triangle, and circle (Figure S16, Supporting Information). By virtue of the high contraction strain generated by SLFs, the resulting single-layer ribbon produced electromechanically bending actuations upon

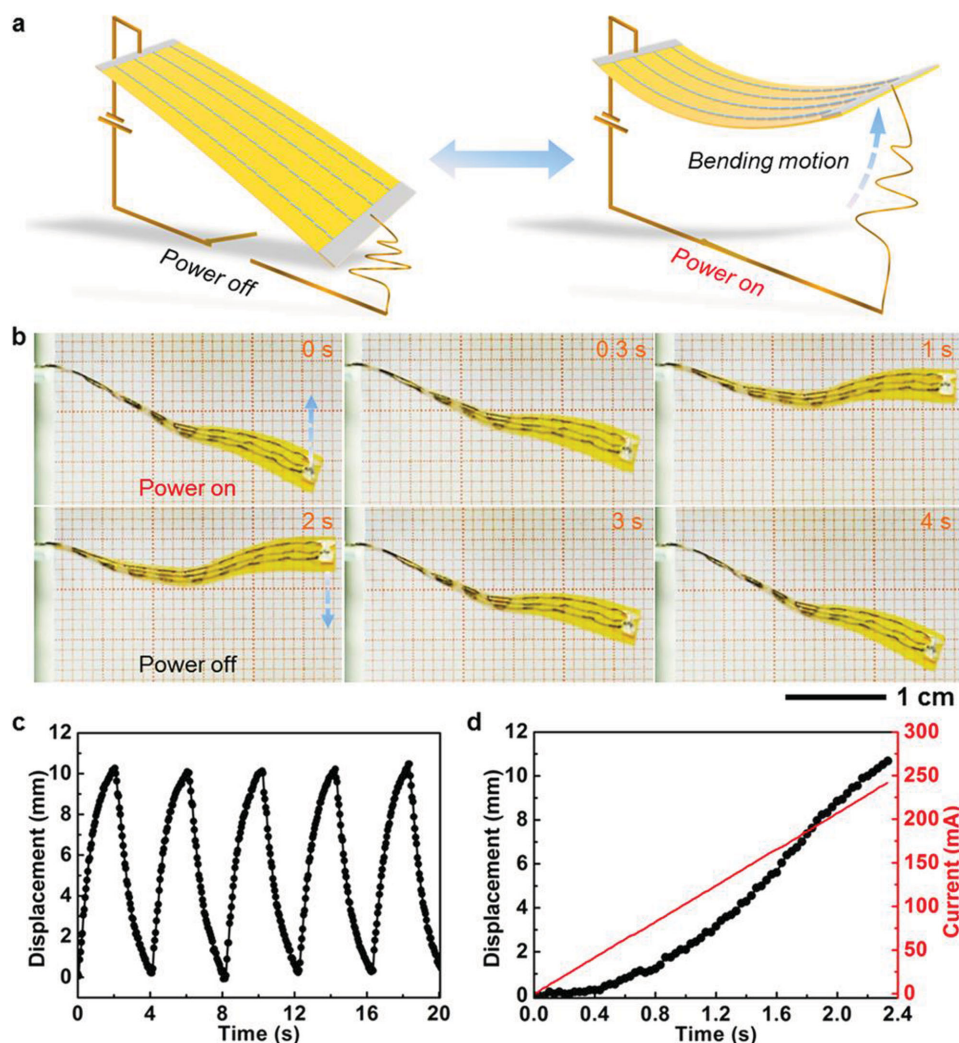


Figure 3. Electromechanically bending motion generated by a Kapton fabric ribbon woven from SLFs. a) Schematic illustration to the experimental setup. b) Photographs of electromechanically bending motions generated by a Kapton ribbon upon applying a pulse current. c,d) Dependence of ascending distance generated by the end of the fabric ribbon on time upon application of a pulse and linear current, respectively. The pulse current shared a magnitude of 240 mA and frequency of 0.25 Hz, and the scan rate of the linear current was $\approx 104 \text{ mA s}^{-1}$.

pass of an electric current and returned to the original state upon removal of the electric current (Figure 3a and Movie S4, Supporting Information). The motion trail under a pulse current of 0.25 Hz was further traced through a frame-by-frame analysis (Figure 3b,c). The free end of the ribbon was raised by $\approx 9 \text{ mm}$ within 1 s, indicating a rapid electromechanical responsiveness. The bending actuations could also be triggered by linear electric currents (Figure 3d). For instance, upon the pass of a linear current with a scan rate of 104 mA s^{-1} , the free end of the ribbon did not generate obvious displacement during the initial 0.5 s while was lifted up beyond the point (Figure 3d), which is consistent with the effect of current magnitude on the electromechanical contraction generated by the woven SLF (Figure S6, Supporting Information). Besides the contractive stress, the left-handed SLF also exerted an anticlockwise torsional force on the Kapton ribbon. However, here no obvious axial torsional motion along the length of the ribbon had been

observed, probably because the generated torsional forces were far from overcoming the in-plane curvature rigidity of the Kapton ribbon.

The fabric ribbon could be shaped into a curved configuration through a heat-setting process to act as an electric walker robot (Figure 4a and Movie S5, Supporting Information). As demonstrated in Figure 4b, upon pass of an electric current, the back end of the walker robot moved forward due to the bending motion generated by the fabric ribbon; once the electric current was disconnected, the back end remained still while the front end shifted forward due to the unbending of the ribbon. Given that, the walker robot thus crawled forward step by step when a continuous pulse current was used. A crawling distance of $\approx 5 \text{ mm}$ had been achieved after pass of six cycles of pulse currents (Figure 4c). In principle, the crawling frequency and stride of the walker robot can be readily tuned by varying the frequency and magnitude of pulse current besides its structure optimization.

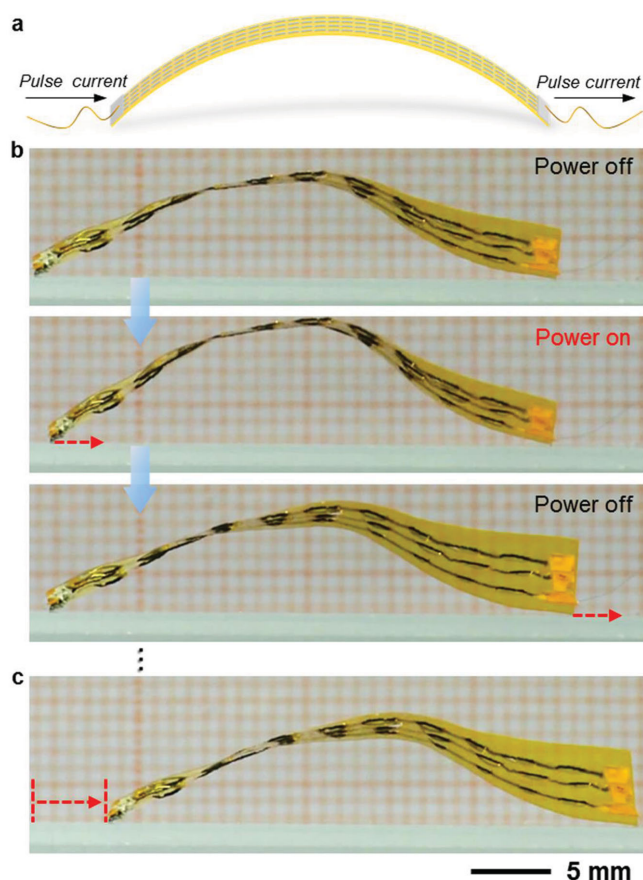


Figure 4. Crawling motion generated by an electric walker robot. a) Schematic illustration to the experimental setup. b) Photographs of a walker robot crawling on a substrate upon pass and removal of the electric current. c) Photograph of the walker robot after pass of six cycles of pulse currents (240 mA and 0.25 Hz).

The SLF-integrated Kapton fabric ribbons could be further designed into a helically 3D configuration (Figure 5a). To prepare the ribbon helix, a slender fabric ribbon was first helically wound around a fine mandrel and subsequently underwent a heat-setting treatment. The left- and right-handed helices were obtained by changing the winding direction of slender fabric ribbons during the preparation process. For simplicity, the left and right-handed helical ribbons derived from SLFs with a left-handed chirality had been mainly studied below. Interestingly, opposite electromechanical contraction (Figure 5b,c, Movie S6, Supporting Information) and elongation (Figure 5c,d, Movie S7, Supporting Information) motions were generated from the left and right-handed helix ribbons, respectively. When a pulse current (80 mA and 0.25 Hz) was passed through the SLF in a left-handed ribbon, a rapid contraction of $\approx 20\%$ in length was generated within 900 ms and reached a maximal value of 24% (Figure 5f). The response speed is one or two orders of magnitude faster than that of typical electrothermally and electrochemically driven layered actuators.^[8,12] In contrast, a rapid elongation of 26% was generated from the right-handed helix

ribbon under the same pulse current. The electromechanical motions could be also triggered by linear electric currents; thus, the generated strain rates could be accurately tuned by varying the scan rates of the currents (Figure 5g). At present, most traditional layered actuators are suffered from the drawbacks including short cycle life and inferior actuation stability, e.g., electrochemical actuators generally exhibited irreversible actuations after tens of cycles due to the evaporation or electrolysis of electrolyte.^[10,11] However, by virtue of the electromechanical stability for the SLFs, the contractive actuation generated by the ribbon helix was highly reversible, and no obvious decrease in contractive strain had been observed after 1000 cycles of actuation (Figure 5h). Besides the contractive and elongate actuations, the ribbon helix had simultaneously generated rotary actuation upon the pass of electric current (Movies S6 and S7, Supporting Information). Such helical motions are similar to the well-known motions generated by the chiral climbing tendrils upon their swelling and deswelling responses to the moisture, but the electromechanically elongate strain generated by the ribbon helix is two times higher than that of a dry tendril after being immersed in water, accompanied with a much faster mechanical responsiveness.^[36,37]

Note that the same left-handed SLFs were used to prepare the actuating ribbons; thus, the contractive and elongate motions above might be attributable to the chirality of the ribbon. For the 3D helix, the out-plane curvature rigidity was weak and far less than the in-plane curvature rigidity of the ribbon itself. As shown in Figure S17 (Supporting Information), a left-handed SLF generated an anticlockwise rotation upon pass of a current, and thus exerted an anticlockwise torsional force to the ribbon helices. For the left-handed ribbon helix, the helical pitch was decreased due to the anticlockwise torsion of the ribbon that provided by the integrated SLF with the same left-handed chirality (Figure S17b, Supporting Information), i.e., an electromechanical contraction in length was generated. In contrast, due to the mismatch of chirality between the ribbon helix and woven SLF, an opposite lengthwise elongation was produced by a right-handed ribbon helix (Figure S17c, Supporting Information). In consideration of that, electromechanical contraction and elongation could also be tuned by changing the chirality of the integrated SLFs (Figure S18, Supporting Information). For instance, right-handed ribbon helices integrated with left- and right-handed SLFs had generated lengthwise elongation and contraction, respectively (Figures S19 and S20, Supporting Information). In a word, the programmable actuations above could be readily modulated by matching/mismatching of the helical chirality between ribbon helices and SLFs, i.e., a lengthwise contraction would be generated if the ribbon helix and the woven SLFs shared the same chirality, while an elongation generated otherwise, which is consistent with the thermally driven contraction and expansion generated by the polymer coiled fibers with homochiral and heterochiral configurations, respectively.^[38]

In summary, different from the conventional electromechanical actuators based on a multilayered structure, electrically conducting spring-like fibers twisted from aligned CNT fibers are neatly woven into polymer ribbons to prepare

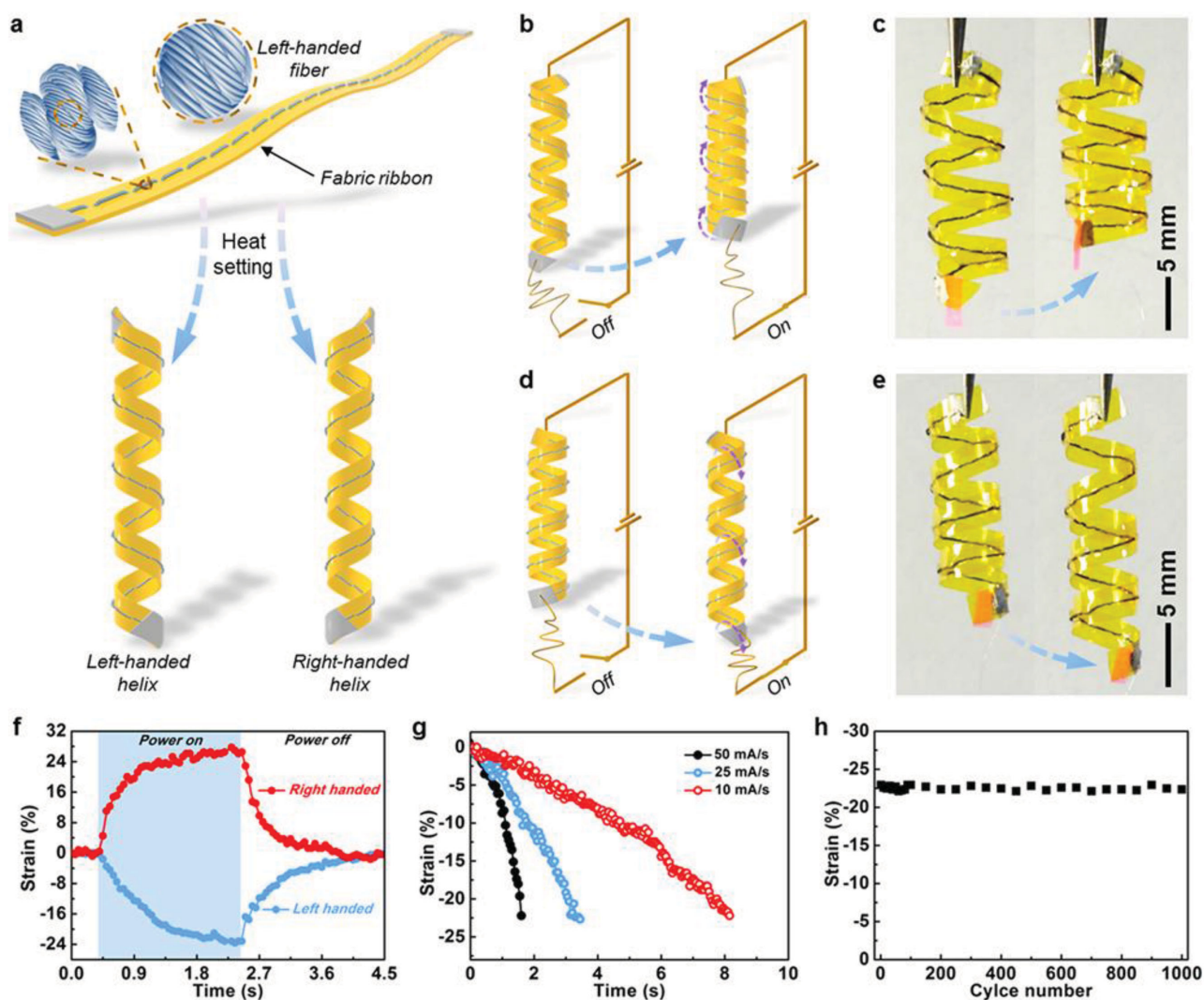


Figure 5. Programmable electromechanical motions generated by helical Kapton fabric ribbons. a) Schematic illustration to the preparation of helical Kapton fabric ribbons with an opposite helical chirality. b,c) Schematic illustration and photographs of the electromechanical contraction motion generated by a left-handed Kapton fabric ribbon, respectively. d,e) Schematic illustration and photographs of the electromechanical elongation motion generated by a right-handed Kapton fabric ribbon, respectively. f) Dependence of electromechanically contractive (black line) and elongate (red line) strain on the time upon application of a pulse current (80 mA and 0.25 Hz), respectively. g) Dependence of electromechanically contractive strain on the time upon application of a linear current with increasing scan rates of 10, 25, and 50 mA s⁻¹. h) Electromechanically contractive strains in 1000 cycles when a pulse current (80 mA and 0.25 Hz) was passed through the left-handed Kapton fabric ribbon.

single-layer actuators with marked electromechanical performances. The fabric ribbons have been further designed into helically 3D structures to generate lengthwise contraction or elongation besides the typical bending/unbending deformation in planar ribbons. The programmable actuations are rapid, reversible, operated by low voltage (<10 V cm⁻¹) and can be well repeated for thousands of cycles without fatigue. This work represents an efficient route to developing high-performance actuating materials and devices by designing hierarchical structures.

Experimental Section

Experimental details are included in the Supporting Information.

Supporting Information

Supporting Information is available from the Wiley Online Library or from the author.

Acknowledgements

P.C. and S.H. contributed equally to this work. This work was supported by MOST (2011CB932503), NSFC (21225417), STCSM (12nm0503200, 15XD1500400), the Fok Ying Tong Education Foundation, the Program for Special Appointments of Professors at Shanghai Institutions of Higher Learning, and the Program for Outstanding Young Scholars from the Organization Department of the CPC Central Committee.

Received: April 13, 2015

Revised: May 15, 2015

Published online: July 20, 2015

- [1] J. D. Madden, *Science* **2007**, *318*, 1094.
- [2] R. H. Baughman, *Science* **2005**, *308*, 63.
- [3] Y. Huang, J. Liang, Y. Chen, *J. Mater. Chem.* **2012**, *22*, 3671.
- [4] X. Zhao, Q. Wang, *Appl. Phys. Rev.* **2014**, *1*, 021304.
- [5] D. B. Li, W. F. Paxton, R. H. Baughman, T. J. Huang, J. F. Stoddart, P. S. Weiss, *MRS Bull.* **2009**, *34*, 671.
- [6] Q. Zhou, S. Lau, D. Wu, K. K. Shung, *Prog. Mater. Sci.* **2011**, *56*, 139.
- [7] J. J. Liang, L. Huang, N. Li, Y. Huang, Y. P. Wu, S. L. Fang, J. Oh, M. Kozlov, Y. F. Ma, F. F. Li, R. Baughman, Y. S. Chen, *ACS Nano* **2012**, *6*, 11097.
- [8] C. Jo, D. Pugal, I.-K. Oh, K. J. Kim, K. Asaka, *Prog. Polym. Sci.* **2013**, *38*, 1037.
- [9] P. Brochu, Q. Pei, *Macromol. Rapid Commun.* **2010**, *31*, 10.
- [10] L. Kong, W. Chen, *Adv. Mater.* **2014**, *26*, 1025.
- [11] T. Mirfakhrai, J. D. W. Madden, R. H. Baughman, *Mater. Today* **2007**, *10*, 30.
- [12] F. Carpi, R. Kornbluh, P. Sommer-Larsen, G. Alici, *Bioinspir. Biomim.* **2011**, *6*, 045006.
- [13] Q. Li, C. Liu, Y. H. Lin, L. Liu, K. Jiang, S. Fan, *ACS Nano* **2015**, *9*, 409.
- [14] R. Pelrine, *Science* **2000**, *287*, 836.
- [15] J. F. Zang, S. Ryu, N. Pugno, Q. M. Wang, Q. Tu, M. J. Buehler, X. H. Zhao, *Nat. Mater.* **2013**, *12*, 321.
- [16] J. Rödel, W. Jo, K. T. P. Seifert, E.-M. Anton, T. Granzow, D. Damjanovic, *J. Am. Ceram. Soc.* **2009**, *92*, 1153.
- [17] X. M. Sun, T. Chen, Z. B. Yang, H. S. Peng, *Acc. Chem. Res.* **2013**, *46*, 539.
- [18] Q. W. Li, X. F. Zhang, R. F. DePaula, L. X. Zheng, Y. H. Zhao, L. Stan, T. G. Holesinger, P. N. Arendt, D. E. Peterson, Y. T. Zhu, *Adv. Mater.* **2006**, *18*, 3160.
- [19] M. Zhang, K. R. Atkinson, R. H. Baughman, *Science* **2004**, *306*, 1358.
- [20] M. F. De Volder, S. H. Tawfik, R. H. Baughman, A. J. Hart, *Science* **2013**, *339*, 535.
- [21] H. Peng, *Fiber-Shaped Energy Harvesting and Storage Devices*, Springer, Berlin, Germany, **2015**.
- [22] J. Foroughi, G. M. Spinks, G. G. Wallace, J. Oh, M. E. Kozlov, S. Fang, T. Mirfakhrai, J. D. Madden, M. K. Shin, S. J. Kim, R. H. Baughman, *Science* **2011**, *334*, 494.
- [23] M. D. Lima, N. Li, M. Jung de Andrade, S. Fang, J. Oh, G. M. Spinks, M. E. Kozlov, C. S. Haines, D. Suh, J. Foroughi, S. J. Kim, Y. Chen, T. Ware, M. K. Shin, L. D. Machado, A. F. Fonseca, J. D. Madden, W. E. Voit, D. S. Galvao, R. H. Baughman, *Science* **2012**, *338*, 928.
- [24] J. Yuan, P. Poulin, *Science* **2014**, *343*, 845.
- [25] W. Guo, C. Liu, F. Zhao, X. Sun, Z. Yang, T. Chen, X. Chen, L. Qiu, X. Hu, H. Peng, *Adv. Mater.* **2012**, *24*, 5379.
- [26] F. Meng, X. Zhang, R. Li, J. Zhao, X. Xuan, X. Wang, J. Zou, Q. Li, *Adv. Mater.* **2014**, *26*, 2480.
- [27] P. Chen, Y. Xu, S. He, X. Sun, W. Guo, Z. Zhang, L. Qiu, J. Li, D. Chen, H. Peng, *Adv. Mater.* **2015**, *27*, 1042.
- [28] L. Qiu, X. Sun, Z. Yang, W. Guo, H. Peng, *Acta Chim. Sin.* **2012**, *70*, 1523.
- [29] H. S. Peng, X. M. Sun, F. J. Cai, X. L. Chen, Y. C. Zhu, G. P. Liao, D. Y. Chen, Q. W. Li, Y. F. Lu, Y. T. Zhu, Q. X. Jia, *Nat. Nanotechnol.* **2009**, *4*, 738.
- [30] J. Kim, B. Kang, *Smart Mater. Struct.* **2001**, *10*, 750.
- [31] Y. Fang, T. J. Pence, X. B. Tan, *IEEE ASME T. Mech.* **2011**, *16*, 656.
- [32] N. Plaza, S. L. Zelinka, D. S. Stone, J. E. Jakes, *Smart Mater. Struct.* **2013**, *22*, 072001.
- [33] H. Therien-Aubin, Z. L. Wu, Z. Nie, E. Kumacheva, *J. Am. Chem. Soc.* **2013**, *135*, 4834.
- [34] Z. J. Wei, Z. Jia, J. M. Athas, C. Y. Wang, S. R. Raghavan, T. Li, Z. H. Nie, *Soft Matter* **2014**, *10*, 8157.
- [35] Z. L. Wu, M. Moshe, J. Greener, H. Therien-Aubin, Z. Nie, E. Sharon, E. Kumacheva, *Nat. Commun.* **2013**, *4*, 1586.
- [36] S. J. Gerbode, J. R. Puzey, A. G. McCormick, L. Mahadevan, *Science* **2012**, *337*, 1087.
- [37] J. S. Wang, G. Wang, X. Q. Feng, T. Kitamura, Y. L. Kang, S. W. Yu, Q. H. Qin, *Sci. Rep.* **2013**, *3*, 3102.
- [38] C. S. Haines, M. D. Lima, N. Li, G. M. Spinks, J. Foroughi, J. D. Madden, S. H. Kim, S. Fang, M. Jung de Andrade, F. Goktepe, O. Goktepe, S. M. Mirvakili, S. Naficy, X. Lepro, J. Oh, M. E. Kozlov, S. J. Kim, X. Xu, B. J. Swedlove, G. G. Wallace, R. H. Baughman, *Science* **2014**, *343*, 868.